DOI: 10.1002/ ((adma.201804801R1))
Article type: Communication

Large electro-optical effect through electrostriction in a nano-mechanical metamaterial

Artemios Karvounis, Behrad Gholipour, Kevin F. MacDonald, and Nikolay I. Zheludev*

Dr. A. Karvounis, Dr. B. Gholipour, Prof. K. F. MacDonald, and Prof. N. I. Zheludev
Optoelectronics Research Centre and Centre for Photonic Metamaterials, University of Southampton, Southampton, SO17 1BJ, UK
E-mail: ak1c13@soton.ac.uk
Dr. B. Gholipour
Department of Chemistry, University of Southampton, Southampton, SO17 1BJ, UK
Prof. N. I. Zheludev
Centre for Disruptive Photonic Technologies & The Photonics Institute, School of Physical and Mathematical Sciences, Nanyang Technological University, Singapore 637371

Keywords: photonic metamaterials; electrostriction; electro-optic modulation; nano-mechanics

Electrostriction is a property of all naturally occurring dielectrics whereby they are mechanically deformed under the application of an electric field. Here we demonstrate that an artificial metamaterial nanostructure comprising arrays of dielectric nano-wires, made of silicon and indium tin oxide, is reversibly structurally deformed under the application of an electric field, and that this reconfiguration is accompanied by substantial changes in optical transmission and reflection, thus providing a strong electro-optic effect. Such metamaterials can be used as the functional elements of electro-optic modulators in the visible to near-infrared part of the spectrum: We demonstrate a modulator operating at 1550 nm with effective electrostriction and electro-optic coefficients of order 10^{-13} m^2V^{-2} and 10^{-6} mV^{-1} respectively. Transmission changes of up to 3.5% are obtained with a 500 mV control signal at a modulation frequency of ~6.5 MHz. With a resonant optical response that can be spectrally tuned by design, modulators based on the artificial electrostrictive effect may be used for laser Q-switching and mode-locking among other applications that require modulation at megahertz frequencies.

In regard to the pervasive technological challenge of electrically controlling (i.e. modulating/routing) guided and free-space optical signals (at macro-, micro-, and lately nano-scopic scales), mechanisms for electrically switching and tuning the optical properties of bulk or thin film media and surfaces have been the subject of research interest over many decades: The Kerr and Pockels electro-optic effects are widely used in amplitude, phase and polarization modulators; carrier-induced changes in doped semiconductors are harnessed in optoelectronic and silicon photonic devices;[1] Liquid crystals reliant electric field-induced molecular reorientation, acousto-optic modulators and micro-electro-mechanical systems, MEMS are the foundation of numerous display, spatial light modulation and adaptive optics technologies. [2–6]

In recent years, photonic metamaterials – manmade media with nanostructurally engineered optical properties[7,8] – have emerged as an enabling technology platform within which all kinds of light-matter interaction can be resonantly enhanced and dynamically controlled. Large electro-optic, EO effects have been demonstrated over extremely short, subwavelength, interaction lengths through the hybridization of active media, including semiconductors,[9,10] graphene,[11–13] phase-change materials,[14–17] and liquid crystals,[18,19] with plasmonic metamaterials.[20] Indeed, the latter can also provide unique (e.g. electro-magneto-optical) response functions that have no counterpart in bulk optical media. In these nano-electro-mechanical structures, Coulomb and Lorentz forces are harnessed to manipulate the conformation of constituent plasmonic metal unit cell elements fabricated on flexible dielectric nano-membranes, the elastic deformation of which provides the necessary restoring force.

‘All-dielectric’ metamaterials are typically manufactured from high-index, low-loss media such as silicon and rely upon the excitation of displacement current, as opposed to plasmonic, resonances.[21–26] They have attracted considerable attention of late, not least for their potential to mitigate the drawbacks associated with plasmonic metal architectures in various

applications at optical frequencies. However, while their optical properties are readily amenable to active control via hybridization,[27] macroscopic substrate deformation, [28] phase-change,[29,30] and photo-excitation [31,32] (including nanostructural reconfiguration induced by optical forces[33]), in being characteristically comprised of discrete dielectric or semiconductor 'particles' they are not immediately suited to delivering nano-electro-mechanical optical switching/tuning functions. Here we report on the realization of a free-standing, all-dielectric, metamaterial EO modulator in which indium tin oxide (ITO) is employed as a transparent, low-index conductor in tandem with nanostructured silicon, to enable low-power modulation of near-infrared transmission at MHz frequencies via electrostrictive nano-mechanical reconfiguration. Silicon, as the archetypal high-index, low-loss platform for optical-frequency all-dielectric metamaterials[22-24] provides the resonant optical response necessary to enhance low-voltage modulation contrast, while ITO, as perhaps the best-known member of the conductive oxide family (which also includes Al- and Ga-doped zinc oxides) provides conductivity for electrostatic actuation without introducing the optical losses that would come with use of a metal.

Electrostriction is a property of all bulk dielectrics, arising from a quadratic coupling between strain and electric field, which manifests itself as a small field-induced mechanical deformation dependent upon the magnitude but not the polarity of the field. The largest electrostrictive coefficients reaching ~10^{-16} m^2/V^2 are found in certain ceramics[34,35] and polymers,[36–40] which have been investigated for potential applications ranging from sonar and high-precision positional actuation [41,42] to MEMS textile fibers.[43] Recent analytical and computational studies have considered the enhancement of electrostriction in artificial composite metamaterials comprising metal, dielectric or semiconductor nanoparticles embedded in a dielectric matrix. [44,45] In the present case, the electric-field-induced deformation of the metamaterial unit cell structure is driven by Maxwell stress [46,47] – specifically the electrostatic force between neighboring, oppositely charged nanowires,

providing a resonantly enhanced effective electrostriction coefficient of order 10^{-13} m^2V^{-2}, and an associated EO coefficient of ~10^{-6} mV^{-1}.

The metamaterial EO modulator in **Figure 1** comprises an array of nanowires with length L = 18 μm manufactured on a free-standing bilayer membrane of silicon and ITO, see Methods, with each period containing an asymmetric pair of closely spaced Si/ITO strips-one being wider than the other. The optical response of the nanowire array is predominantly determined by the structural geometry of the high-refractive-index silicon component. Dimensions are selected here, for a bilayer of h_1 = 100 nm Si and h_2 = 70 nm ITO, to achieve transmission/reflection resonances in the near-infrared telecommunications band around 1550 nm (**Figure 2**): a sub-wavelength period P = 800 nm, nanowire widths $w_{1,2}$ = 200, 300 nm, and a gap sizes d_1 = 100 nm, which leaves a gap d_2 = 200 nm between neighboring pairs of nanowires. The ITO layer meanwhile provides electrical connectivity to facilitate electrostatic tuning of the gap sizes. For this purpose, the ITO layer is patterned at each end of the nanowires such that neighboring pairs are electrically isolated from each other and connected to opposing terminals of the device, i.e. such that alternate pairs are alternately biased as annotated in Figure 1b.

Normal incidence reflection and transmission spectra for the metamaterial device are measured using a microspectrophotometer, see Methods. For TE-polarized light, incident electric field parallel to the nanowires, the metamaterial presents a Fano-type resonant response as shown in Figure 2a, with a quality factor Q~35. This is based upon the excitation of anti-parallel displacement currents in the dimensionally asymmetric nanowire pairs,[48,49] predominantly within the silicon, as illustrated by the numerically simulated cross-sectional field maps in Figure 2b. In contrast, spectra for the orthogonal, TM-polarization are essentially flat, with transmission >80% and reflection ~10% across the entire near-IR spectral range.

The resonant optical properties of the Si/ITO metamaterial are strongly dependent on the nanowire pair separation $d_{1,2}$, which can be continuously and to a point reversibly controlled by applying an electrical bias. In the ++-- configuration indicated in Figure 1b, the nanowires in each asymmetric pair are subject to electrostatic forces of mutual repulsion and (more weakly by virtue of greater separation) of attraction to the nearest neighboring wires of the adjacent pairs. In consequence, the two nanowires in each pair move away from one another, increasing the gap size d_1 and decreasing d_2. This nano-mechanical reconfiguration red shifts the TE resonance, leading to changes in transmission and reflection that are most pronounced where the dispersion is steepest.

We first evaluate induced changes in transmission as a function of applied DC bias. **Figure 3**a presents the spectral dispersion of relative transmission change $\Delta T/T_0$, where $\Delta T = T_\alpha - T_0$; T_α being the absolute transmission at an applied bias of α Volts. At 2V bias the induced change reaches maximum values of +7% and -4% at wavelengths of 1497 and 1544 nm, either side of 1520 nm the zero-bias transmission resonance wavelength. 2V represents a conservative upper limit on the operational range of applied bias within which electrostatic control of nanowire separation provides continuous and reversible tuning of transmission. Beyond this, there comes a point at which the elastic restoring force on a nanowire (which increases linearly with displacement from its equilibrium position, i.e. with increasing gap size d_1) is surpassed by the electrostatic force of attraction to its oppositely biased neighbor (which grows as d_2^{-2}; see Figures 3b, c). At this point the gap will abruptly close and, by virtue of Van der Waals forces, remain closed even when the applied bias is removed. An order-of-magnitude estimate for this irreversible switching threshold can be obtained analytically[50] (assuming a symmetric pair of beams in a material with Young's modulus E) as $\alpha^* \approx \sqrt{32Ehw^3d^2/(\pi\varepsilon_o L^4)}$, and is found experimentally for the present sample geometry to be ~3V. The change in transmission associated with this irreversible deformation of the

metamaterial structure (i.e. reduction of gap size d_2 to zero) is unsurprisingly much larger than those observed within the reversible tuning range, as illustrated by the vertically-scaled dashed line in Figure 3a.

For the purposes of studying the high-frequency AC EO modulation characteristics of the Si/ITO metadevice, the metamaterial is mounted in a low-vacuum microscope stage to reduce air-damping of induced nanowire oscillations, see Methods. The relative change in metadevice transmission is monitored at a fixed wavelength of 1550 nm while varying the frequency f of an applied sinusoidal electrical bias with an amplitude α of up to 500 mV, **Figure 4**. At low frequencies the induced displacement of the nanowires, and therefore the magnitude of the induced change in transmission, is small. Both however are enhanced when the nanowires are driven at their natural mechanical resonance frequency: in the present case, $\Delta T/T_0$ reaches 3.5% at a frequency of 6 MHz (as compared to only ~0.5% off resonance) at a drive amplitude of 500 mV. Transmission modulation amplitude increases super-linearly with drive voltage as shown in the inset to Figure 4. One might anticipate the presence of a double peak in the frequency spectrum, by virtue of the fact that there are nanowires with two different widths (and therefore Eigenfrequencies) within each unit cell of the metamaterial. From numerical simulations, employing Young's Moduli E and densities ρ for Si and ITO from Refs. [51,52], these frequencies are estimated to be 4.07 and 6.10 MHz for the 200 and 300 nm wide nanowires respectively. The observation of a single peak, extending at FWHM from 5.7 to 6.8 MHz, is attributed to the coupled nature of the oscillations (which may include components of out-of-plane and twisting motion) stress within the bilayer derived from the Si membrane fabrication and/or ITO annealing processes, and to spectral broadening associated with manufacturing imperfections of up to 10% variation in $w_{1,2}$ over the metamaterial array. The nano-mechanical functionality of the metamaterial can be understood as a form of artificial electrostriction at the unit cell level, in that it comprises a structural deformation dependent upon the magnitude of an applied electric field E. Specifically, strain s should

exhibit a quadratic dependence on the applied field: $s = ME^2$, where M is the electrostrictive coefficient. (In bulk materials M is a fourth ranked tensor; here we evaluate what, in these terms, would be the longitudinal electrostriction coefficient M_{11} under an assumption that the applied field, resulting stress and deformation are all unidirectional and parallel.)

We quantify strain as the change Δd in the size of the gaps between Si/ITO nanowires (the magnitude of the increase in d_1 or decrease in d_2), relative to the mean equilibrium gap size $\bar{d}=(d_1^*+d_2^*)/2$, where $d_{1,2}^*$ are the zero-bias gap sizes of 100 and 200 nm respectively in the present case. Numerical simulations demonstrate that for small values of Δd metamaterial optical transmission is, to a very good approximation, a linear (of course spectrally dispersive) function of strain in these terms, as illustrated in **Figure 5**a. Experimentally measured dependences of transmission upon applied bias α can thus be translated into dependences, Figure 5b of strain upon applied electric field $E = \alpha/\bar{d}$, from which effective electrostriction coefficients for both DC and AC modes of excitation can be derived.

The metamaterial's DC effective electrostriction coefficient is found to be $M_{DC} = 4 \times 10^{-18}$ m^2V^{-2} – a value somewhat smaller than the largest coefficients found in bulk dielectric media.[39,53] However, this value is enhanced by five orders of magnitude when the structure is driven in AC mode at its mechanical resonance frequency, reaching $M_{AC} = 3 \times 10^{-13}$ m^2V^{-2}, a value three orders of magnitude larger than can be found in bulk dielectrics. It should further be noted that these represent conservative estimates of the electrostriction coefficients: strain is underestimated because higher resonance quality factors in simulation as compared to experiment exaggerate the dependence of transmission upon strain and electric fields are overestimated, the bias applied to the device terminals is assumed across the gaps between nanowires with no account taken of ohmic losses in the ITO.

The change in optical properties brought about by the electrostrictive deformation of the metamaterial can be described by an effective electro-optic coefficient $r = \Delta nL/\alpha$, where Δn is

the effective refractive index change induced over an interaction length L (the thickness of the metamaterial, $h_1 + h_2 = 170$ nm) under an applied bias of α V. Numerical simulations indicate a phase shift in transmission at 1550 nm of up to $\pi/9$ at a nanowire displacement $\Delta d = 3$ nm (strain of 2%, achieved at a DC bias of 2V). This corresponds to an effective index change $\Delta n \sim 0.5$, giving $r \approx 10^{-6}$ mV^{-1} - a value approximately five orders of magnitude larger than in typical electro-optic media such as lithium niobate (3×10^{-11} mV^{-1}).[54]

In summary, we have demonstrated a free-standing, all-dielectric metamaterial electro-optic modulator of substantially sub-wavelength thickness ($<\lambda/8$), manufactured from CMOS-compatible (high-index low-loss semiconductor and transparent conductive oxide) materials. The device provides continuous and reversible electrically-actuated nano-mechanical tuning of near-infrared transmission, at wavelengths selected by design, presenting effective electrostriction and electro-optic coefficients orders of magnitude larger than those of bulk dielectric media: Electrostatic forces are harnessed to control the separation between elements of a non-diffractive Si/ITO nanowire array and so to deliver, in the present case, relative transmission changes of up to 7% at 1550 nm under an applied DC bias of 2V. In this low frequency limit, power consumption is dominated by leakage resistance of 500 kΩ and amounts to only 8 μW at a bias of 2V. In AC mode, optical modulation amplitude is enhanced when structures are driven at their few-MHz mechanical resonance frequencies. Depending on application requirements, an appropriate balance among modulation amplitude, power consumption and speed of response may be engineered: For example, longer nanowires would have a lower mechanical resonance frequency but they would be displaced further at a given a given bias voltage than shorter wires, producing a larger change in transmission. Greater modulation contrast may be achieved via optimization of the metamaterial nanofabrication procedure, enhancement of both optical and mechanical resonance quality factors by reduction of dimensional inhomogeneity.

Experimental section

Metamaterial fabrication: Devices are manufactured on commercially sourced polycrystalline silicon membranes (1 mm × 1 mm windows supported in 200 μm thick silicon frames). These are coated (including the frame) with 70 nm of indium tin oxide by radio-frequency sputtering from an In_2O_3/SnO_2 (90/10 wt%) alloy target. A base pressure of 4×10^{-5} mbar was achieved before deposition and a high-purity argon gas flow of 70 ccpm was used to strike the plasma. A 20:5 argon: oxygen deposition gas mixture was used to maintain the plasma and ensure sufficient oxygen content in the deposited ITO film. The membrane substrate was held on a rotating platen approximately 150 mm from the target where it is subject to a temperature increase of <10°C during deposition, ensuring minimal stress in the film, which was subsequently annealed at 200°C for 60 minutes under an oxygen atmosphere to increase conductivity (measured sheet resistance decreases from 3.4×10^6 to 1×10^3 Ω/sq; carrier concentration increases from 3.5×10^{16} cm^{-3} to 10^{21} cm^{-3}).

Metamaterial arrays of asymmetric nanowire pairs were fabricated by focused ion beam (FIB) milling from the ITO side of the bilayer membrane, cutting through both layers of material. The pattern of electrodes required to alternately bias pairs of nanowires (as indicated in Figure 1b) was then defined by FIB milling in the ITO layer only.

Numerical simulations: Full-wave electromagnetic simulations of the metamaterial structure, based on the geometry presented in Figure 1c, were performed using the finite element method in COMSOL Multiphysics. Calculations employ periodic boundary conditions in the *x* and *y* directions (i.e. effectively assuming an infinite array of infinitely long nanowires). They utilize refractive indices for polycrystalline silicon and for ITO from ellipsometric measurements (both materials have weakly dispersive indices in the near-IR spectral range above ~1300 nm: 3.45 + 0.005i for Si and 1.9 + 0.08i for ITO), and assume normally incident, narrowband, linearly polarized plane wave illumination.

The electrostatic field distribution and its dependence on gap sizer, as presented in Figures 3b and 3c, were modelled using the AC/DC COMSOL module, assuming a pair of parallel, free-standing 18 μm long wires, with the ITO surface of one held uniformly at a given bias voltage against the other at 0V (ground).

Nanowire mechanical Eigenfrequencies are obtained from finite element models of single, isolated wires of 18 μm length with fixed ends and rectangular cross sections as presented in Figure 1c. These assume Young's Moduli E and density ρ values for Si and ITO [51,52]: E_{Si} = 150, E_{ITO} = 190 GPa; ρ_{Si} =2300, ρ_{ITO} = 7300 kg.m^{-3}.

Microspectrophotometry (including DC EO modulation measurements): Transmission and reflection spectra (Figure 2) were obtained using a microspectrophotometer (CRAIC QDI2010), with a 15 μm × 15 μm sampling aperture via a 15× objective with NA 0.28. All data are normalized to reference levels for air (100% transmission), a silver mirror (high reflector) and a 'Vantablack' vertically-aligned carbon nanotube array (zero reflection/transmission), and averaged over 15 repeated measurement cycles, each with a 500 ms integration time. For DC EO characterization, a source measure unit (Keithley 2636) was employed to apply a DC bias across the metadevice terminals.

High-frequency EO modulation measurements: The metamaterial sample was mounted in a low-vacuum (~1 mbar) microscope stage equipped with an RF electrical feedthrough via which a control bias signal from an electrical network analyzer (Agilent Technologies E5071C) could be applied to the metadevice terminals. Optical transmission was monitored at a wavelength of 1550 nm using a diode laser providing a CW intensity of 70 μW/cm^2 at the sample and an InGaAs photodetector (New Focus 1811) connected to the network analyzer. Data are averaged over five frequency scans at each setting of peak bias voltage; Error bars in the inset to Figure 4 are calculated as the standard error.

Acknowledgements

This work was supported by the UK Engineering and Physical Sciences Research Council [grants EP/M009122/1 and EP/N00762X/1] and the Singapore Ministry of Education [grant MOE2016-T3-1-006]. We thank J. Y. Ou for assistance with electro-optical measurements and M. E. Rizou for helpful discussions.

Received: ((will be filled in by the editorial staff))

Revised: ((will be filled in by the editorial staff))

Published online: ((will be filled in by the editorial staff))

References

[1] G. T. Reed, G. Mashanovich, F. Y. Gardes, D. J. Thomson, *Nat. Photonics* **2010**, *4*, 518.

[2] E. A. Donley, T. P. Heavner, F. Levi, M. O. Tataw, S. R. Jefferts, *Rev. Sci. Instrum.* **2005**, *76*, 063112.

[3] T. Bifano, *Nat. Photonics* **2011**, *5*, 21.

[4] W. M. Zhu, A. Q. Liu, T. Bourouina, D. P. Tsai, J. H. Teng, X. H. Zhang, G. Q. Lo, D. L. Kwong, N. I. Zheludev, *Nat. Commun.* **2012**, *3*, 1274.

[5] Z. Zhang, Z. You, D. Chu, *Light Sci. Appl.* **2014**, *3*, e213.

[6] K. Shih, P. Pitchappa, M. Manjappa, C. P. Ho, R. Singh, B. Yang, N. Singh, C. Lee, *Appl. Phys. Lett.* **2017**, *110*, 161108.

[7] N. I. Zheludev, Y. S. Kivshar, *Nat. Mater.* **2012**, *11*, 917.

[8] A. M. Urbas, Z. Jacob, L. D. Negro, N. Engheta, A. D. Boardman, P. Egan, A. B. Khanikaev, V. Menon, M. Ferrera, N. Kinsey, C. DeVault, J. Kim, V. Shalaev, A. Boltasseva, J. Valentine, C. Pfeiffer, A. Grbic, E. Narimanov, L. Zhu, S. Fan, A. Alù, E. Poutrina, N. M. Litchinitser, M. A. Noginov, K. F. MacDonald, E. Plum, X. Liu, P.

F. Nealey, C. R. Kagan, C. B. Murray, D. A. Pawlak, I. I. Smolyaninov, V. N. Smolyaninova, D. Chanda, *J. Opt.* **2016**, *18*, 93005.

[9] D. J. Cho, W. Wu, E. Ponizovskaya, P. Chaturvedi, A. M. Bratkovsky, S.-Y. Wang, X. Zhang, F. Wang, Y. R. Shen, *Opt. Express* **2009**, *17*, 17652.

[10] K. M. Dani, Z. Ku, P. C. Upadhya, R. P. Prasankumar, S. R. J. Brueck, A. J. Taylor, *Nano Lett.* **2009**, *9*, 3565.

[11] A. E. Nikolaenko, N. Papasimakis, E. Atmatzakis, Z. Luo, Z. X. Shen, F. De Angelis, S. A. Boden, E. Di Fabrizio, N. I. Zheludev, *Appl. Phys. Lett.* **2012**, *100*, 181109.

[12] J. Li, P. Yu, H. Cheng, W. Liu, Z. Li, B. Xie, S. Chen, J. Tian, *Adv. Opt. Mater.* **2016**, *4*, 91.

[13] Z. Li, W. Liu, H. Cheng, S. Chen, J. Tian, *Opt. Lett.* **2016**, *41*, 3142.

[14] M. J. Dicken, K. Aydin, I. M. Pryce, L. A. Sweatlock, E. M. Boyd, S. Walavalkar, J. Ma, H. A. Atwater, *Opt. Express* **2009**, *17*, 18330.

[15] Z. L. Sámson, K. F. MacDonald, F. De Angelis, B. Gholipour, K. Knight, C. C. Huang, E. Di Fabrizio, D. W. Hewak, N. I. Zheludev, *Appl. Phys. Lett.* **2010**, *96*, 143105.

[16] A. K. U. Michel, D. N. Chigrin, T. W. W. Maß, K. Schönauer, M. Salinga, M. Wuttig, T. Taubner, *Nano Lett.* **2013**, *13*, 3470.

[17] R. F. Waters, P. A. Hobson, K. F. MacDonald, N. I. Zheludev, *Appl. Phys. Lett.* **2015**, *107*, 081102.

[18] A. Minovich, J. Farnell, D. N. Neshev, I. McKerracher, F. Karouta, J. Tian, D. A. Powell, I. V. Shadrivov, H. Hoe Tan, C. Jagadish, Y. S. Kivshar, *Appl. Phys. Lett.* **2012**, *100*, 121113.

[19] O. Buchnev, J. Y. Ou, M. Kaczmarek, N. I. Zheludev, V. a Fedotov, *Opt. Express* **2013**, *21*, 1633.

[20] N. I. Zheludev, E. Plum, *Nat Nano* **2016**, *11*, 16.

[21] P. Moitra, Y. Yang, Z. Anderson, I. I. Kravchenko, D. P. Briggs, J. Valentine, *Nat.*

Photonics **2013**, *7*, 791.

[22] S. Jahani, Z. Jacob, *Nat. Nanotechnol.* **2016**, *11*, 23.

[23] A. I. Kuznetsov, A. E. Miroshnichenko, M. L. Brongersma, Y. S. Kivshar, B. Lukyanchuk, *Science.* **2016**, *354*, aag2472.

[24] I. Staude, J. Schilling, *Nat. Photonics* **2017**, *11*, 274.

[25] O. Yavas, M. Svedendahl, P. Dobosz, V. Sanz, R. Quidant, *Nano Lett.* **2017**, *17*, 4421.

[26] A. Karvounis, V. Nalla, K. F. MacDonald, N. I. Zheludev, *Adv. Mater.* **2018**, *30*, 1707354.

[27] J. Sautter, I. Staude, M. Decker, E. Rusak, D. N. Neshev, I. Brener, Y. S. Kivshar, *ACS Nano* **2015**, *9*, 4308.

[28] P. Gutruf, C. Zou, W. Withayachumnankul, M. Bhaskaran, S. Sriram, C. Fumeaux, *ACS Nano* **2016**, *10*, 133.

[29] A. Karvounis, B. Gholipour, K. F. Macdonald, N. I. Zheludev, **2016**, *109*, 051103.

[30] B. Gholipour, A. Karvounis, J. Yin, C. Soci, K. F. MacDonald, N. I. Zheludev, *NPG Asia Mater.* **2018**, *10*, 533.

[31] M. R. Shcherbakov, P. P. Vabishchevich, A. S. Shorokhov, K. E. Chong, D. Y. Choi, I. Staude, A. E. Miroshnichenko, D. N. Neshev, A. A. Fedyanin, Y. S. Kivshar, *Nano Lett.* **2015**, *15*, 6985.

[32] Y. Yang, W. Wang, A. Boulesbaa, I. I. Kravchenko, D. P. Briggs, A. Puretzky, D. Geohegan, J. Valentine, *Nano Lett.* **2015**, *15*, 7388.

[33] A. Karvounis, J. Y. Ou, W. Wu, K. F. Macdonald, N. I. Zheludev, *Appl. Phys. Lett.* **2015**, *107*, 191110.

[34] K. N. Pham, A. Hussain, C. W. Ahn, W. Kim, S. J. Jeong, J. S. Lee, *Mater. Lett.* **2010**, *64*, 2219.

[35] F. Li, L. Jin, Z. Xu, S. Zhang, *Appl. Phys. Rev.* **2014**, *1*, 011103.

[36] W. Lehmann, H. Skupin, C. Tolksdorf, E. Gebhard, R. Zentel, P. Krüger, M. Lösche, F.

Kremer, *Nature* **2001**, *410*, 447.

[37] F. Bauer, E. Fousson, Q. M. Zhang, *IEEE Trans. Dielectr. Electr. Insul.* **2006**, *13*, 1149.

[38] V. V. Kochervinskiĭ, *Crystallogr. Reports* **2009**, *54*, 1146.

[39] B. Kim, Y. D. Park, K. Min, J. H. Lee, S. S. Hwang, S. M. Hong, B. H. Kim, S. O. Kim, C. M. Koo, *Adv. Funct. Mater.* **2011**, *21*, 3242.

[40] M. Lallart, P. J. Cottinet, D. Guyomar, L. Lebrun, *J. Polym. Sci. Part B Polym. Phys.* **2012**, *50*, 523.

[41] J. Galvagni, *Opt. Eng.* **1990**, *29*, 1389.

[42] A. Kholkin, B. Jadidian, A. Safari, *Ceramics, Piezoelectric and Electrostrictive*, Encycl. Smart Mater., John Wiley & Sons, Inc., **2002**.

[43] T. Khudiyev, J. Clayton, E. Levy, N. Chocat, A. Gumennik, A. M. Stolyarov, J. Joannopoulos, Y. Fink, *Nat. Commun.* **2017**, *8*, 1435.

[44] M. J. A. Smith, B. T. Kuhlmey, C. M. De Sterke, C. Wolff, M. Lapine, C. G. Poulton, *Phys. Rev. B.* **2015**, *91*, 214102.

[45] A. Singh, M. J. A. Smith, C. Martin De Sterke, *J. Opt. Soc. Am. B* **2017**, *34*, 1573.

[46] J. Li, N. Rao, *Appl. Phys. Lett.* **2002**, *81*, 1860.

[47] B. Guiffard, L. Seveyrat, G. Sebald, D. Guyomar, *J. Phys. D. Appl. Phys.* **2006**, *39*, 3053.

[48] V. V Khardikov, E. O. Iarko, S. L. Prosvirnin, *J. Opt.* **2012**, *14*, 35103.

[49] B. Zeng, A. Majumdar, F. Wang, *Opt. Express* **2015**, *23*, 12478.

[50] J.-Y. Ou, E. Plum, J. Zhang, N. I. Zheludev, *Nat. Nanotechnol.* **2013**, *8*, 252.

[51] W. N. Sharpe, B. Yuan, R. Vaidyanathan, R. L. Edwards, *Proc. Tenth IEEE Int. Work. Microelectromechanical Syst.* **1997**, *429*, 424.

[52] B. Lee, Y. Song, J. Yoon, *2009 IEEE 22nd Int. Conf. Micro Electro Mech. Syst.* **2009**, 148.

[53] R. Korobko, A. Patlolla, A. Kossoy, E. Wachtel, H. L. Tuller, A. I. Frenkel, I. Lubomirsky, *Adv. Mater.* **2012**, *24*, 5857.

[54] E. K. Turner, *IEEE J. Quantum Electron.* **1966**, *2*, 128.

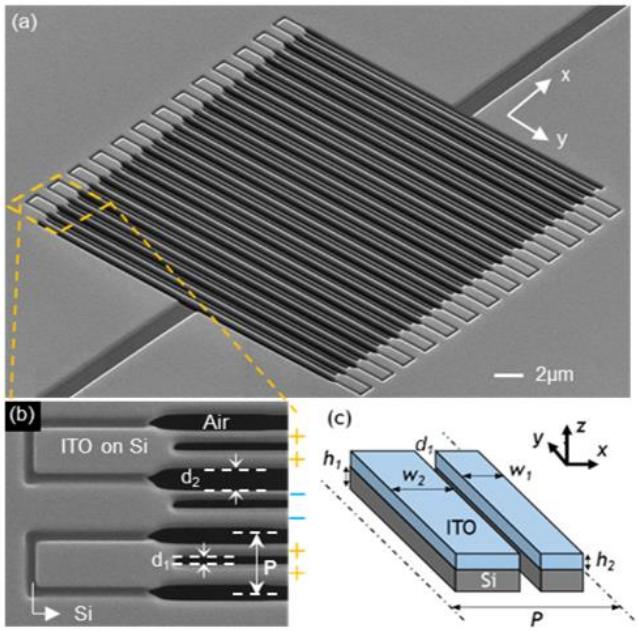

Figure 1. All-dielectric, nano-mechanical, metamaterial electro-optic modulator. (a) Scanning electron microscope image of a nanowire array metamaterial manufactured on a silicon/ITO bilayer membrane; (b) shows detail of the structure at the ends of the nanowires; (c) Schematic cross-section of the asymmetric Si/ITO nanowire pair within each period of the metamaterial array [P = 800, h1 = 100, h2 = 70, w1 = 200, w2 = 300, d1 = 100 nm, d2 = 200 nm].

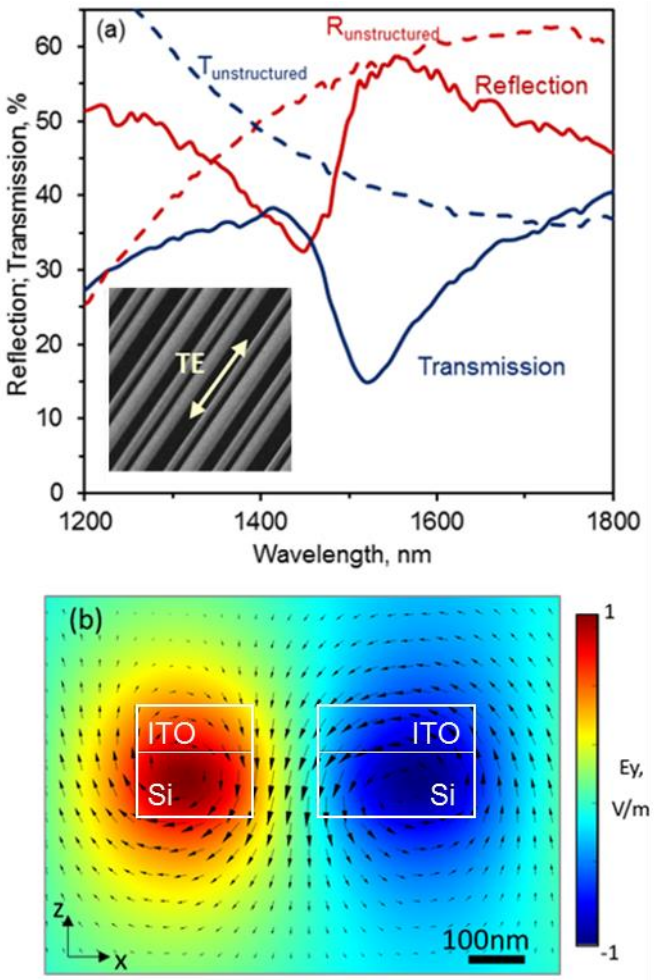

Figure 2. Optical characteristics of the Si/ITO nanowire metamaterial. (a) Measured transmission [solid blue line] and reflection [solid red line] spectra of the Si/ITO nanowire metamaterial shown in Figure 1 for TE-polarized light and corresponding [polarization independent] spectra for the unstructured Si/ITO bilayer [dashed lines]. (b) Numerically simulated distribution of the *y*-component of electric field in the *xz* plane, overlaid with arrows denoting the direction and magnitude of magnetic field, for one pair of asymmetric width nanowires as described in Figure 1b, at the 1520 nm transmission resonance wavelength.

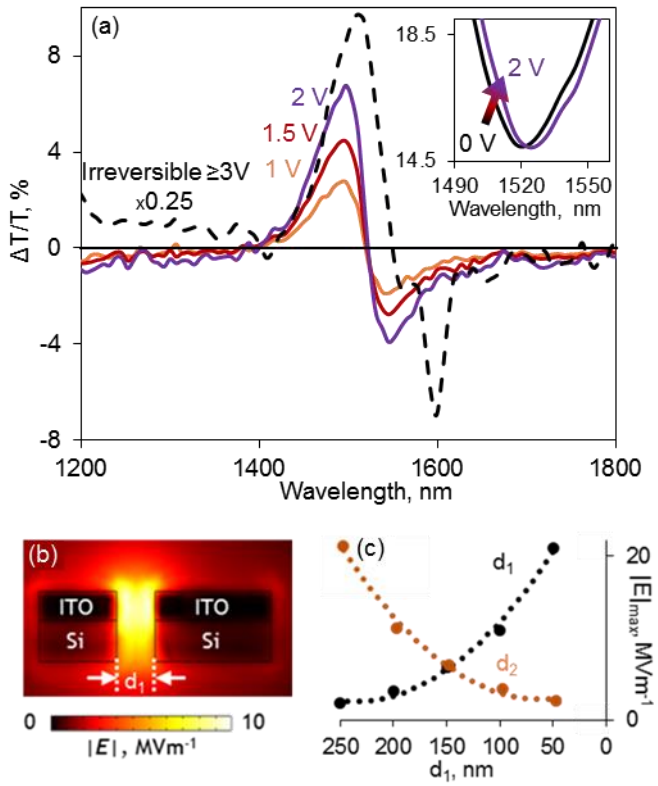

Figure 3. EO tuning of Si/ITO metamaterial transmission. Spectral dispersion of the relative change in transmission of the Si/ITO nanowire metamaterial for a selection of applied DC electrical bias levels [as labelled]. The inset shows the spectral dispersion of absolute transmission around the resonant wavelength for zero and 2V bias settings. (b) Numerically simulated cross-sectional map in the xz plane of the static electric field amplitude over a single period of the metamaterial array for a gap size d_1 = 100 nm and an applied bias of 1V between the ITO sections of the two nanowires. (c) Maximum electric field amplitude [at the midpoint of the gap between the nanowires] as a function of gap size, for a fixed 1V bias.

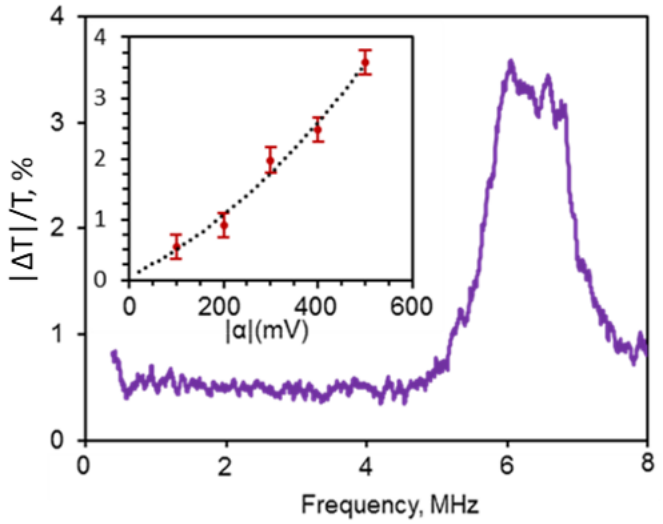

Figure 4. Dynamic electro-optic modulation of Si/ITO metamaterial transmission. Relative change in transmission at 1550 nm of the Si/ITO nanowire metamaterial shown in Figure 1 as a function of the drive voltage modulation frequency, for a fixed peak bias α = 500 mV. The inset shows the peak magnitude of induced transmission change at 6 MHz as a function of peak bias voltage *α*.

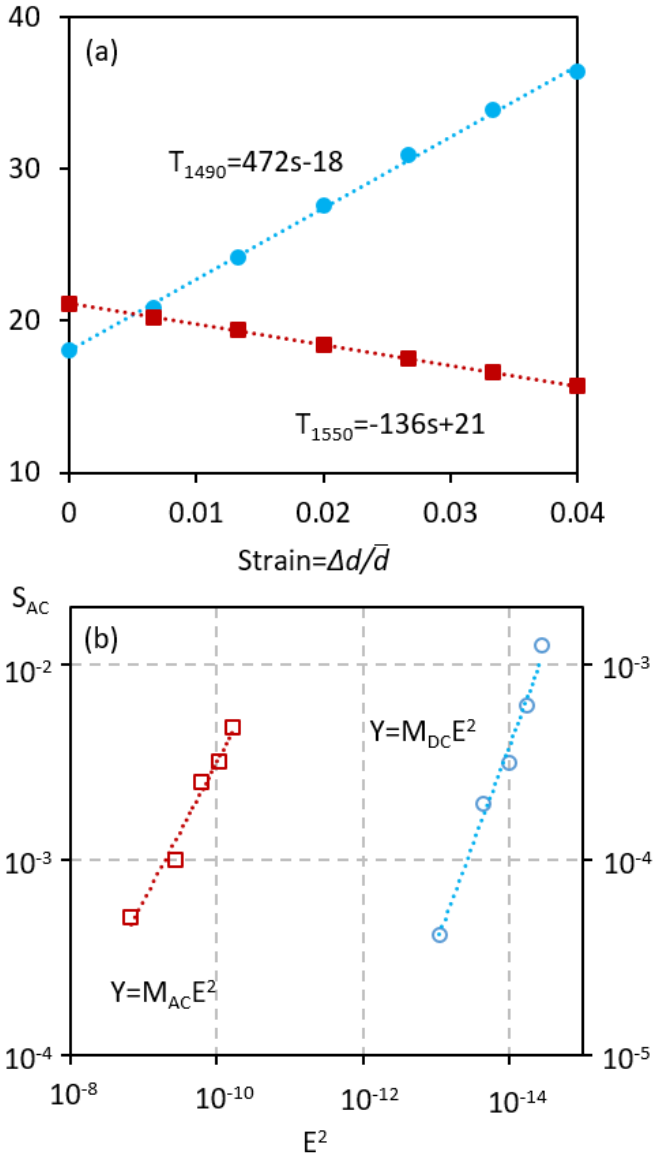

Figure 5. Si/ITO metamaterial electrostriction. (a) Numerically simulated spectral dispersion of Si/ITO nanowire metamaterial transmission as a function of strain, defined as the relative change in the size of the gaps between nanowires, for wavelengths of 1490 (blue) and 1550 nm (red) at which maximally positive and negative proportionalities are observed. (b) Strain induced within the metamaterial structure [from experimental measurements of optical transmission at 1490 nm for DC bias and 1550 nm for AC bias, via proportionalities derived from panel (a)] as a function of applied DC and peak AC (f = 6 MHz) electric field squared.

We demonstrate a nano-mechanical metamaterial providing electro-optic modulation via electrostriction. The modulator, which comprises arrays of bilayer silicon/indium-tin-oxide nano-wires that are reversibly deformed under the application of an electric field, operates at 1550 nm with effective electrostriction and electro-optic coefficients orders of magnitude larger than those of bulk dielectrics (reaching 10^{-13} m^2V^{-2} and 10^{-6} mV^{-1} respectively).

Keywords: photonic metamaterials; electrostriction; electro-optic modulation; nano-mechanics

A. Karvounis*, B. Gholipour, K. F. MacDonald, and N. I. Zheludev

Large electro-optical effect through electrostriction in a nano-mechanical metamaterial